

Journal of Biomedical Optics

BiomedicalOptics.SPIEDigitalLibrary.org

Transducer-matched multipulse excitation for signal-to-noise ratio improvement in diode laser-based photoacoustic systems

Maxim N. Cherkashin
Carsten Brenner
Martin R. Hofmann

SPIE.

Maxim N. Cherkashin, Carsten Brenner, Martin R. Hofmann, "Transducer-matched multipulse excitation for signal-to-noise ratio improvement in diode laser-based photoacoustic systems," *J. Biomed. Opt.* **24**(4), 046001 (2019), doi: 10.1117/1.JBO.24.4.046001.

Transducer-matched multipulse excitation for signal-to-noise ratio improvement in diode laser-based photoacoustic systems

Maxim N. Cherkashin,* Carsten Brenner, and Martin R. Hofmann

Ruhr University Bochum, Photonics and Terahertz Technology, Faculty of Electrical Engineering and Information Technology, Bochum, Germany

Abstract. We analyze transducer-matched multipulse excitation as a method for improving of the signal-to-noise ratio (SNR) for diode laser-based photoacoustic systems. We discuss the principle of the technique, its advantages, and potential drawbacks and perform measurements to analyze the obtainable SNR increase. We show in experiment and computationally that a lower boundary estimate of 1.2 to 1.8 fold SNR improvement can be provided using transducer-matched pulse bursts, depending on the transducer and particular arrangement. Finally, we analyze implications that the transducer resonance effects may have on the recently introduced advanced photoacoustic techniques. The findings are of immediate interest to modalities utilizing dense pulse sequences and systems possessing limited pulse energy. In particular, transducer-matched multipulse excitation may be beneficial for diode-based photoacoustic systems operated with transducers in the range of 1 to 5 MHz since the required hardware is readily available. © The Authors. Published by SPIE under a Creative Commons Attribution 4.0 Unported License. Distribution or reproduction of this work in whole or in part requires full attribution of the original publication, including its DOI. [DOI: [10.1117/1.JBO.24.4.046001](https://doi.org/10.1117/1.JBO.24.4.046001)]

Keywords: photoacoustic imaging; diode lasers; ultrasound transducers; resonance; signal-to-noise ratio.

Paper 180672R received Dec. 19, 2018; accepted for publication Mar. 19, 2019; published online Apr. 9, 2019.

1 Introduction

Diode lasers (DLs) are compact, easy-to-use, and low maintenance laser sources. They offer a possibility to operate with high modulation frequencies and almost arbitrary on/off patterns. These advantages make DLs interesting candidates for compact photoacoustic imaging (PAI) systems. However, the critical drawback, impeding further development of DL-based systems, is their comparably low single-pulse energy. This leads to small signal-to-noise ratios (SNR) that can be achieved practically. In the past couple of decades, a lot of effort was made to find strategies to increase the SNR in DL-based PAI systems. In the following, we outline the different effects of the laser pulse width and pulse-to-pulse distance (or pulse repetition frequency) on signal strength in PAI. As the general photoacoustic equation states,^{1,2} time-variant light flux is required to produce a compression-rarefaction wave, which necessitates the usage of either pulsed or modulated CW light sources. We focus our considerations on pulsed lasers as light sources. However, the discussion presented below can be adapted for other suitable systems without the loss of validity.

The strength of the registered photoacoustic signal is determined by the interactions of the light pulse, the absorber, embedded in the tissue, and the transducer(s) picking up the ultrasonic wave. To understand the dynamics of this complex interaction, each element of the chain can be characterized by one or multiple time constants. Their mutual relationships will determine the systems' operation regime.

Typically, photoacoustic signal theory describes laser pulse width t_p , a characteristic time constant of the light source, in comparison with two temporal constants of the absorber—the

so-called stress relaxation time t_S and the thermal relaxation time t_H . However, for finite absorbers of PAI concern, the combination of their size, speed of sound, and thermal diffusivity leads to $t_S \ll t_H$. Therefore, for our analysis, we will consider t_S the respective characteristic of the absorber and refer to it hereafter as t_A . On the detection side, the ultrasonic transducer can be characterized with its relaxation time t_T . It is possible, therefore, to perform a pairwise or multibody comparison of the mentioned time constants to analyze the dynamics of the system and its operation regimes, and to identify the governing conditions for them to occur. In the following, we systematically examine selected possible permutations of the system time constants and the effects their relations enforce. In this analysis, we focus our attention on the interplay effects rather than the advantages or disadvantages of particular implementations.

1.1 Single-Pulse Photoacoustic Excitation

In the case of so-called delta-pulse excitation, which is most commonly used, the following relations hold: $t_p < t_A < t_T$, the light pulse width is smaller than the other time constants (see Fig. 1 and Table 1, PAT|R). In this regime, the amplitude of the registered PA signal is linearly dependent on the light pulse energy.¹⁻³ For DLs operated in the gain-switched regime, the output pulse energy is proportional to the amount of carriers injected into the active region. However, it can only be increased in a limited range due to intrinsic limitations, therefore, constraining the maximum pulse energy available.

On the other hand, unlike solid-state lasers, laser diodes enable a wide range pulse width adjustment. Therefore, elongated pulses can be utilized in attempt to increase the SNR. In this case, the absorber is faster than the light pulse, and the following relations hold: $t_A < t_p < t_T$ (see Fig. 1 and Table 1, APT|R). One special case that should be mentioned is a bandwidth-matched

*Address all correspondence to Maxim N. Cherkashin, E-mail: maxim.cherkashin@rub.de

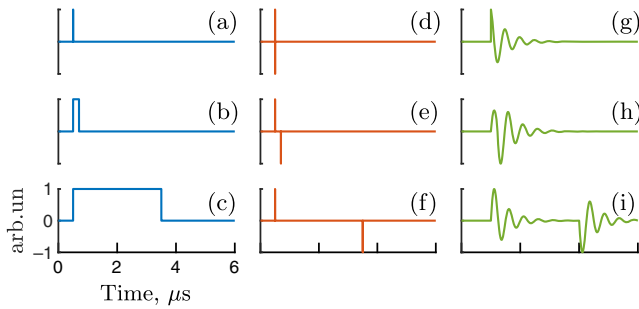


Fig. 1 Schematic representation of the (a)–(c) light intensity, (d)–(f) absorber, and (g)–(i) transducer responses for the single-pulse excitation cases listed in Table 1. Rows represent consecutively regimes (a), (d), (g) PAT|R; (b), (e), (h) APT|R; and (c), (f), (i) ATP|R. All signals are normalized to be vertically within $[-1; 1]$ interval and are consistent over time axis as depicted in (c). The signals are presented for illustrative purposes only and are modeled as following. Absorber response is a differential of light intensity, whereas transducer response is as convolution of the respective absorber signal with a damped oscillation waveform.

condition; when the laser pulse width matches the dynamics of the ultrasonic transducer, $t_p \sim t_T$ (Ref. 5).

When further increasing the pulse width, $t_A < t_T < t_p$, the long pulse regime can be implemented.^{4,8} In this case, the transducer registers separately the acoustic pulses related to the on and offset of the illumination. Moreover, the heat accumulated due to the thermal energy delivered to the absorber with the pulse is affecting its properties. Accordingly, front and back shocks differ from each other⁸ (see Fig. 1 and Table 1, ATP|R).

The cases mentioned so far are utilized with relatively low pulse repetition rate (or long pulse-to-pulse delay time t_R) and are illustrated in Fig. 1 and summarized in Table 1. If the pulse repetition rate, other key characteristic of the light source, is increased, few multipulse excitation regimes can be realized in practice.

1.2 Multiple Pulse Photoacoustic Excitation

First, if short pulses are used with high repetition rate, $t_p < t_R < t_A < t_T$, the absorber is unable to resolve individual

pulses in the train, and the result is effectively linear addition of their pulse energy¹¹ (see Fig. 2 and Table 2, PRAT). Next, once the pulse repetition rate approaches the absorber resonance, $t_R \sim t_A$, its resonant excitation is possible along a range of sizes^{12–15} (Fig. 2 and Table 2, PR \sim AT). To guide the reader on the relevant absorber dimensionality and the resonant frequencies involved, some of the most important cases are listed in Table 3. Further, when the interpulse delay is longer than the transducer relaxation time so that a single pulse can be resolved by the transducer and multiple pulses fit in the acquisition window, $t_p < t_A < t_T < t_R$, coded excitation can be used for SNR improvement^{16–19} (Fig. 2 and Table 2, PATR).

Finally, there is one more special case left. For the condition when the pulse repetition rate approaches the transducer resonance, $t_R \sim t_T$, resonant excitation of the transducer can be performed (Fig. 2 and Table 2, PAR \sim T). In this paper, we analyze the possibility to employ such transducer-matched multipulse photoacoustic excitation (TM-MPE) for SNR improvement in the DL-based PAI systems and discuss the implications transducer resonance effects might have on the other operation regimes.

2 Transducer-Matched Multipulse Photoacoustic Excitation

2.1 Principle and Physical Basis

Due to the close proximity of the fields, many PAI systems took over transducers developed for pulse-echo ultrasonic (PEU) imaging. Such transducers are engineered for excitation with a short voltage spike. This is analogous to their operation for detection of broadband photoacoustic signals, produced in the delta-pulse excitation regime (see Fig. 1 and Table 1, PAT|R). Motivated by the need of the precise identification of the sources of acoustic inhomogeneities in PEU, these transducers are typically optimized to have larger bandwidth. This is advantageous for PAI since the transducer bandwidth translates in reconstruction procedure into better localization of absorbers spread in the tissue. Additionally, to further improve SNR and reduce artifacts, these transducers are strongly damped to decrease ringing.²¹

Table 1 Light pulse width regimes and effects in PAI, rule <.

Permutation	Description, confinement statement	Observed effect(s)	References
PAT R	Light pulse width is smaller than absorber relaxation time, $t_p < t_A$, δ -pulse excitation regime.	Laser pulse is acting as an instant heat source, SNR is proportional to the pulse energy.	Conventional PAI ^{1–3}
APT R	Light pulse width is longer than absorber relaxation, $t_A < t_p$, typical situation for DL-PAI systems with moderate pulse widths.	Detected PAI signal becomes a convolution of absorber response function with light pulse shape, SNR can be improved with transducer bandwidth-matched pulses.	DL-based PAI systems ^{4–7}
ATP R	Light pulse width is longer than transducer waveform duration, $t_T < t_p$.	Long laser pulse is resolved by transducer as separated onset and offset pulses, which might be different from each other due to the heat accumulated.	DL-based PAI systems, operated in the long pulse regime ^{4,8}

Note: t_p , t_A , t_R , and t_T are the characteristic of laser pulse, absorber, pulse train in multiple pulse excitation experiments, and ultrasonic transducer as parts of PAI signal generation chain, respectively. Left column of the table denotes selected possible permutations of the characteristic times by respective subscripts, with elements having their magnitudes increasing left to right, i.e., PAT $\equiv t_p < t_A < t_T$. Vertical bar denotes that interpulse delay time t_R is larger than the acquisition frame width and is not affecting the dynamics of the system. Permutations with $t_T < t_A$ are omitted since they are not relevant for the absorber sizes of concern and transducer frequencies used. In this limit, the absorber is effectively bearing half-space function; the reader may refer for details to Refs. 3, 9, and 10.

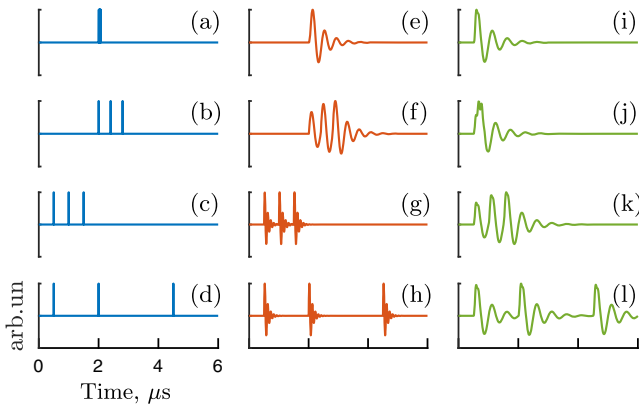


Fig. 2 Schematic representation of the (a)–(d) light intensity, (e)–(h) absorber and (i)–(l) transducer responses for the multiple pulse excitation cases listed in Table 2. Rows represent consecutively regimes (a), (e), (i) PRAT; (b), (f), (j) PR ~ AT; (c), (g), (k) PAR ~ T; and (d), (h), (l) PATR. All signals are normalized to be vertically within $[-1; 1]$ interval and are consistent over time axis as depicted in (d), except (a), (b), (e), and (f), which are time stretched to illustrate the fast phenomena. The signals are presented for illustrative purposes only and are modeled as following. Absorber response is a convolution of light intensity with high-frequency damped oscillation waveform, whereas transducer response is as convolution of the respective absorber signal with a damped oscillation waveform.

Principally, a single-element ultrasonic transducer is a thin stiff disk of piezoelectric material acting as bidirectional pressure–voltage converter. When subjected to the external voltage or pressure, it is involved in a damped oscillation process and is acting, respectively, as a source or receiver of acoustic waves. Such systems, driven with force with a frequency approaching their resonance frequency, should exhibit a nonlinear increase in their oscillation’s amplitude.

In PAI, the photoacoustic pressure, driving the transducer, is the absorber’s response on the deposition of energy by the light pulse. Therefore, in the delta-pulse excitation regime, if the burst of pulses is incident on a small absorber, the transducer shall be subjected to a series of bipolar perturbations. Thus, tuning the pulse repetition frequency (or interpulse delay) to adjust to the

Table 3 Multiscale resonance behavior of selected absorbers in the PAI domain.

Target	Lateral extent	Resonant frequency range	References
Gold nanoparticles	100 s of nm	10 s of GHz	12 and 13
Red blood cells	1 s of μm	1 s of MHz	(Estimate)
Tissue layers	10 s of μm	100 s of KHz	14 and 15

transducers’ frequency shall result in its resonant excitation (see Fig. 2 and Table 2, PAR ~ T).

To examine the effect of the transducer resonance on the maximum registered photoacoustic amplitude, the pulse repetition rate has to be chosen carefully. Considering the range of the values of t_R available, it is instructive to analyze initially the extreme cases. First, the interpulse delay has to be greater than the absorber’s resonant response, $t_R > t_A$, which is valid for the majority of practical situations. If two pulses are close to each other, the Grueneisen relaxation effect may be observed.²² It is nonlinearly dependent on the interpulse delay time and in the limit of small t_R it might cover the transducer resonance. On the other hand, in the absence of the resonant effects, the signals of individual pulses $U_{sp}(t)$ arriving at the transducer with various interpulse delay times shall add linearly^{16,17,23,24}

$$U_{mpl}(t) = U_{sp}(t) + U_{sp}(t + t_R) + \dots, \quad (1)$$

where U_{mpl} is the registered transducer signal for multiple pulse excitation.

In the domain of photoacoustic coded excitation (PACE), the extremes of pulse repetition rate are typically at least a multiple of transducer oscillation period t_T with maximum pulse repetition frequencies up to 1 MHz.^{16–19}

Therefore, the range of the interpulse delay times t_R , where the transducer resonance effects might be observed, is bound in lower limit by stronger Grueneisen relaxation nonlinearity and in higher limit by linear addition as in PACE.

Table 2 Multiple pulse excitation regimes and their effects in PAI, rule <.

Permutation	Description, confinement statement	Observed effects	References
PRAT	Multiple pulse excitation with interpulse delays smaller than absorber response time, $t_R < t_A$, individual pulses are not resolved by absorber.	Single-pulse energy is linearly added, SNR is proportional to total pulse energy (c.f. PAT R).	11
PR ~ AT	Absorber resonance matching is possible when $t_R \sim t_A$.	SNR improvement via nonlinearity of the absorber resonance phenomena.	12–15
PAR ~ T	Multipulse excitation with single laser pulses resolved by absorber, but not necessarily by transducer, $t_R \leq t_T$, resonant transducer excitation is possible when $t_R \sim t_T$.	SNR improvement via TM-MPE.	This paper
PATR	Interpulse delay time is larger than transducer relaxation time; however, multiple pulses are launched within single acquisition frame, $t_T \leq t_R$.	SNR improvement using coded excitation.	16–19

Note: See footnote for Table 1 for description. For a complementary view on a variety of modulation techniques used in PAI, readers may refer to a recent review in Ref. 20.

2.2 Experimental Arrangement

To investigate the TM-MPE, an experimental system capable of adjusting the interpulse delay t_R and the number of pulses in the pulse burst N_p is required. For the double-pulse excitation, it is possible to have a synchronized pair of lasers to perform classic pump-probe investigation.^{12,22} However, scaling the number of pulses in the excitation train can be quite challenging.¹¹ On the other hand, one convenient option is the usage of gain-switched laser diodes, where the on/off patterns can be selected arbitrarily within the parameter range the device could withstand.

Over the course of this study, we have utilized two different illumination sources while the general experimental setting remained the same (Fig. 3). Light from the DL, supplied with current driver (CD) and operated via a control unit (CU) is coupled using the coupling assembly (CA) into the multimode fiber (MMF) and then focused on a target with focusing assembly (FA).

Two illumination configurations are built as follows: (A) 905 nm DL (Laser Components), with driver LDP-V50-100V3 and CU PLCS-21, coupled into 600- μm core MMF, providing 1.2- μJ pulses of 12-ns length²⁵ and (B) custom-build laser diode bar 652 nm (Ferdinand-Braun Institute), with beam transformation optics (BTS series, LIMO), supplied with LDP-V-240-100 and PLCS-20, coupled into 550- μm core MMF, providing 1.1- μJ pulses of 31-ns length.^{23,24} DL drivers (LDP-V*) and CUs (PLCS*) are from PicoLAS.

Blackened plastic foil, used as a target, is immersed in water, together with a single-element ultrasound transducer (UST, see Table 4 for specifications). The detected photoacoustic signals are amplified by a broadband low-noise amplifier (Amp, HSA-Y-1-40, 40-dB gain, Femto) and fed to a digital sampling oscilloscope (DSO, Wavesurfer 104Mx, LeCroy). The data acquisition control and the postprocessing are performed on a PC using MATLAB (MathWorks). Number of pulses N_p and interpulse delays t_R in the excitation sequences are adjusted via trigger signals produced by an arbitrary function generator (AFG, AFG3102, Tektronix).

The experimental data are treated as following. For each N_p -pulse excitation configuration, $N_{\text{acq}} = 100$ consecutive acquisitions of the photoacoustic signal $U_{\text{mpe}}(t, N_p, t_R)$ are performed and, respectively, ensemble averaged. The DC offset is removed by subtracting the mean of signal-free part for each averaged trace. The maximum peak-to-peak signal amplitude

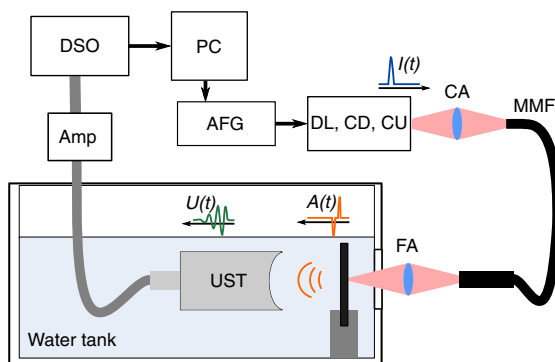


Fig. 3 Schematics of the experimental arrangement. AFG, arbitrary function generator; DL, diode laser; CD, current driver; CU, control unit; CA and FA, coupling and focusing assemblies, respectively; MMF, multimode fiber; UST, ultrasound transducer; Amp, low-noise amplifier; DSO, digital sampling oscilloscope.

Table 4 USTs and illumination sources used in the study.

Type	F_n (MHz)	F_c (MHz)	F_p (MHz)	l_f (mm)	Illumination source
A392S	1	0.98	0.9	—	A
A395S	2.25	2.31	1.81	—	A
C306	2.25	2.49	1.89	45	B
C380	3.5	3.29	2.18	75	A

Note: F_n , F_c , F_p , l_f are the nominal, central frequency, peak frequency, and focal length, respectively, according to the datasheet, manufacturer: Olympus Panametrics-NDT; illumination sources are as following: (A) 905 nm DL (Laser Components), with DL driver LDP-V50-100V3 and CU PLCS-21, coupled into 600- μm core MMF, providing 1.2- μJ pulses of 12-ns length,²⁵ (B) custom-build laser diode bar 652 nm (Ferdinand-Braun Institute), with beam transformation optics (BTS series, LIMO), supplied with LDP-V-240-100 and PLCS-20, coupled into 550- μm core MMF, providing 1.1- μJ pulses of 31-ns length;^{23,24} DL drivers (LDP-V*) and CUs (PLCS*) are from PicoLAS.

$A_{\text{max|mp}}(N_p, t_R)$ is extracted and normalized by the respective single-pulse excitation value $A_{\text{max|sp}}$. Averaged single-pulse excitation signals $U_{\text{sp}}(t)$ are used as input to build modeled responses $U_{\text{mpl}}(t, N_p, t_R)$, following Eq. (1). The maximum peak-to-peak amplitude is extracted from the modeled responses as described above. It is compared with experimental outcomes and analyzed further.

2.3 Results

To investigate the TM-MPE, the dynamics of the double-pulse excitation response has to be analyzed first. Figure 4 illustrates the dependency of the normalized maximum photoacoustic amplitude of the double-pulse excitation $A_{\text{max|dp}}^n$ on the used interpulse delay time t_R , obtained in experiment and modeled using Eq. (1). It is possible to define four regimes of the combination of the individual pulses on the transducer, denoted in

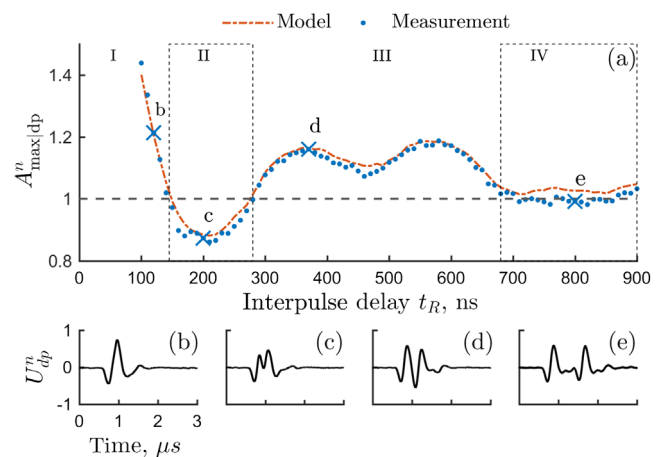


Fig. 4 (a) Interpulse-dependent normalized double-pulse excitation maximum photoacoustic amplitude $A_{\text{max|dp}}^n$, measurement data is shown by points, whereas modeled response is represented by dashed line. C306-type UST data: (b)–(d) normalized RF signals $U_{\text{dp}}^n(t)$, illustrating four operation regimes marked by roman numbers in (a), exact data points marked \times and respective letters (see text for details). The oscillations of $A_{\text{max|dp}}^n$ in the region III are due to the transducer transfer function.²⁴

Fig. 4 with roman numbers and illustrated with a typical signal for each of them.

In the region I, two pulses, even though separated by more than 100 ns, are unresolved by the transducer. In the limit $t_R \rightarrow 0$, with the energy of individual pulses in the μJ range, no significant nonlinear contribution due to Grueneisen relaxation effect²² is added. Then two pulses are essentially merging into one, and the energy of the individual pulses is combined leading to $\lim_{t_R \rightarrow 0} A_{\text{max}|dp}^n = 2$. Therefore, using the interpulse delay t_R in the range I leads to system operation in the collapsed pulse regime, analogous to Fig. 2 and Table 2, PRAT.

Further, in the region II, when the pulse repetition rate is approaching the second harmonic of the transducer resonance frequency or $t_R \sim 0.5t_T$, the signals of individual pulses are combined out-of-phase. This leads to a decrease in the registered maximum amplitude. In this case, the phase cancellation effect occurs, similarly to the results presented in Ref. 26.

Next, in the region III, the pulse repetition rate is within the transducer bandwidth $t_R \sim t_T$, and the signals of individual pulses add in-phase. This leads to an increase in the maximum registered amplitude $A_{\text{max}|dp}^n$. In this region of interpulse delay times, TM-MPE is possible.

Finally, in the region IV, the transducer is able to clearly resolve individual signals. This operation regime is typically used for coded excitation^{16–19} (see Fig. 2 and Table 2, PATR).

Both experimental and simulation results show that maximum peak-to-peak amplitude increases in the regime III (Fig. 4) with double-pulse excitation. To further analyze the extent of this effect, the impact of pulse burst length is examined by varying the number of pulses N_p while the interpulse delay t_R is swept within the range defined by regime III.

To illustrate the dependency of the registered maximum amplitude $A_{\text{max}|mp}^n$ on these parameters, the experimental results are shown in Fig. 5(a), along with the modeled response following Eq. (1) in Fig. 5(b) and their subtraction result in Fig. 5(c). To focus the attention on the stronger deviations between the experimental data and the linear addition model, only the values over the threshold of $\pm 2\text{std}(A_{\text{max}|sp}^n) = \pm 1.9\%$ are shown in the panel (c). This threshold value is taken as a measure of pulse-to-pulse variations.

First, we shall note good general agreement between the measurement outcomes and the linear addition model, following Eq. (1). As the differential image in Fig. 5 suggests, most of the discrepancies are within the measurement error margins. This observation indicates that the contribution of nonlinear effects

in the combination of the single-pulse responses with individual pulse energies in μJ range is relatively small. In this case, it amounts to the maximum of 5% of the maximum amplitude of the single-pulse response $A_{\text{max}|sp}$. The differential image also highlights two positive regions, centered at t_R of 310 and 580 ns, respectively, and spanning $N_p = 2$ to 4. In these regions, the experimentally obtained maximum amplitude exceeds the linear model. Moreover, these are the parameter values, where the relative increase of the registered amplitude is the highest. On the other hand, after $N_p = 5$, the registered maximum photoacoustic amplitude $A_{\text{max}|mp}^n$ saturates. Further increase of the number of pulses in the burst approaches CW excitation of the transducer with the period t_R . It is important to note that with both prominent interpulse delay times a significant part of the increase of the registered amplitude is already achieved with $N_p = 2$.

Additionally, it is noticeable that the double-pulse excitation response differs from responses with $N_p > 2$. In the first case, the maximum registered amplitude $A_{\text{max}|dp}^n$ for interpulse delay times in the range 280 to 350 ns is significantly lower. Increasing the number of pulses in the burst reveals a higher-frequency feature, located approximately at interpulse delay of 310 ns for the transducer shown. This corresponds to a frequency of 3.23 MHz. This is an interesting result since the amplitude transfer function, most often used for the characterization of the transducer output, does not contain this information. Thus, inclusion of the phase transfer function into the analysis might be necessary to explain this behavior.^{24,27}

Based on good overall agreement between the measured double-pulse responses²⁵ and multipulse responses and the linear addition model (Fig. 5), we can use the maximum amplitude of the modeled response to obtain a lower estimate of the impact of the transducer resonance effects on the registered photoacoustic amplitude. Figure 6 shows the modeled influence of the number of pulses in the burst N_p and the interpulse delay t_R on the maximum registered multipulse photoacoustic amplitude $A_{\text{max}|mp}^n$ for a set of the transducers, selected to cover different transducer designs and span a wider frequency range (Table 4).

In agreement with the previous results, multipulse excitation responses of the transducers demonstrate a behavior similar to the one presented in Figs. 4 and 5 in the range of parameters tested. It is notable that the higher-frequency feature, shown in Fig. 5, is present in the modeled multipulse responses of the other transducers used. We stress that such behavior might require the inclusion of the phase transfer function into the analysis,²⁷ even though the number of pulses N_p in the burst

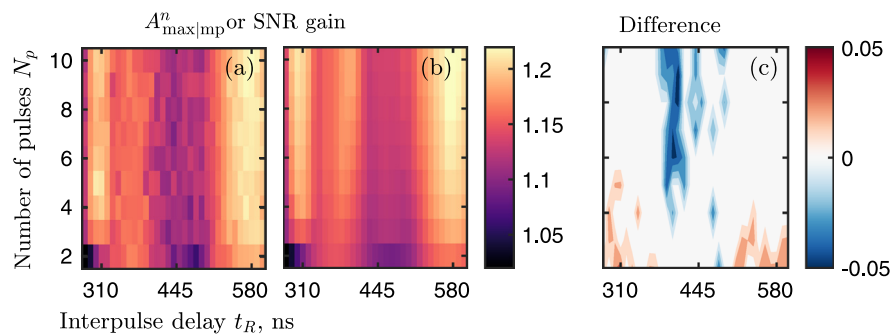


Fig. 5 Interpulse delay t_R and number of pulses N_p -dependent normalized maximum photoacoustic amplitude $A_{\text{max}|mp}^n$: (a) as measured by the C306 type transducer and (b) as provided by linear addition model [Eq. (1)]. (c) Thresholded differential (a) and (b) image. Panels (a) and (b) share the color axis. Following Eq. (2), SNR gain is equal to $A_{\text{max}|mp}^n$. In the panel (c), only the values over the threshold of $\pm 2\text{std}(A_{\text{max}|sp}^n) = \pm 1.9\%$ are shown to highlight the stronger differences between (a) and (b).

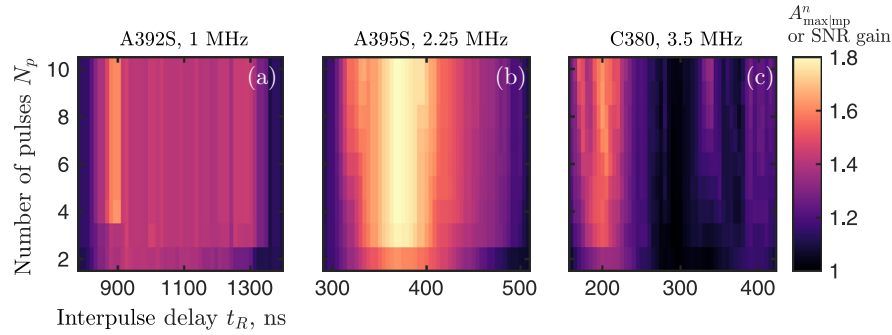


Fig. 6 Modeled influence of the interpulse delay t_R and number of pulses N_p on the normalized maximum photoacoustic amplitude $A_{\max|mp}^n$, for a few selected USTs: (a) A392S, (b) A395S, and (c) C380 (see Table 4 for the transducer specifications). Panels (a)–(c) share the color axis. Interpulse delays t_R are adjusted to cover the central frequency of the given transducer. Following Eq. (2), SNR gain is equal to $A_{\max|mp}^n$.

is relatively small. Additionally, it is important to note that the twin resonance structure of the transfer functions of the C-type transducers translates well in the multipulse excitation response results in agreement with our previous observations.²⁴

Summarizing the results presented in Figs. 4–6, the TM-MPE is providing the 1.2 to 1.8 fold increase in the maximum registered amplitude, dependent on the transducer and particular arrangement used. The SNR in PAI can be calculated as ratio of the signal amplitude to the noise level^{4,16}

$$\text{SNR} = A_{\max}/\sigma, \quad (2)$$

where σ is the noise variance. Therefore, if σ is preserved among single- and multipulse excitation, the SNR gain for TM-MPE is equal to the respective normalized maximum amplitude $A_{\max|mp}^n$ increase (Figs. 5 and 6).

To illustrate the outcomes that the usage of TM-MPE could have, let us analyze a few possible application scenarios. First, in the extreme time-tight case (A), when only single acquisition could be performed, using TM-MPE provides SNR gain equal to the normalized peak-to-peak amplitude $A_{\max|mp}^n$. Given the proportionality of the photoacoustic signals to the light pulse energy, this outcome is analogous to increasing the pulse energy by the same factor. For the systems with limited maximum pulse energy as DLs, it is therefore providing a way to increase the SNR of the signals obtained beyond the device capabilities.

Next, if multiple acquisitions N_{acq} can be performed, TM-MPE can be combined with ensemble averaging in various ways. The two methods rely on the different mechanisms of the SNR improvement. Ensemble averaging makes use of the statistical properties of the noise in the acquired signals and over N_{acq} acquisitions improves SNR by a factor of $\sqrt{N_{\text{acq}}}$.^{4,16} On the other side, TM-MPE is based upon the prior knowledge about the particular UST in use. Therefore, it leads to a direct increase of the maximum registered amplitude. The SNR gain for the TM-MPE is equal to the normalized maximum amplitude increase $A_{\max|mp}^n$ and is transducer dependent. When used in combination (B), the SNR gain factors of two methods multiply [Eq. (2)], as illustrated in Fig. 7.

Finally, the total number of acquisitions N_{acq} can be split to obtain, respectively, two images (e.g., $N_p = 1$ and $N_p = 2$ to 4) with $N_{\text{acq}}/2$ signals for averaging each. This allows acquiring both single- and multipulse frames for advanced processing methods (C). We shall note that, for the transducers demonstrating $A_{\max|mp}^n > \sqrt{2}$, the combination of TM-MPE and averaging

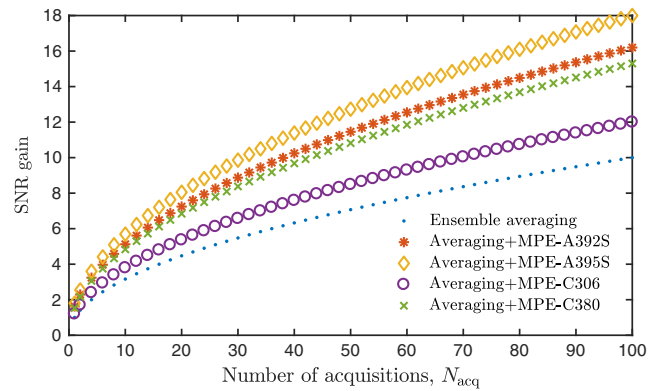


Fig. 7 SNR gain dependence on the number of acquisitions N_{acq} performed for the transducers used in the study for ensemble averaging and averaging in combination with transducer-matched multipulse excitation with $N_p = 4$.

outperforms simple averaging of all N_{acq} signals using only a half of the total acquisitions. Therefore, applying TM-MPE in combination with averaging can provide an alternative to increase SNR over the same total acquisition time, maintain SNR and speed up the signal registration, or maintain the total acquisition time while extracting additional information using both single- and multipulse frames.^{15,28}

3 Discussion and Outlook

In this paper, we investigated the possibility to use the transducer-matched resonant multipulse photoacoustic excitation to improve the SNR in the limited pulse energy PAI systems. We concentrated our analysis on low pulse energy DL-based setups. Our investigation showed that, within mentioned constraints, the individual signals add linearly with their respective interpulse delays. They can be treated in the time domain and might require inclusion of the phase transfer function of the transducer used in the analysis to adequately describe the behavior of the transducer output in the frequency domain. We obtained a 1.2 to 1.8 fold SNR gain due to TM-MPE experimentally and computationally.

In our analysis, we have focused on the maximum amplitude projection approach in PAI. Alternatively, another signal processing technique can be applied, benefiting from the deterministic components of the multipulse excitation responses. However, this extends beyond the scope of our project.

As the differential images in Fig. 5 suggest, the nonlinear contribution in the registered multipulse signal is relatively small. This result is in agreement with the theoretical expectations, considering the pulse energies used in our study and strong damping of the USTs. Even though V-type USTs are often preferred in PAI for their optimization on axial resolution, we focused on A-type and C-type transducers. In the frequency range of this study, the bandwidth of all three transducer types does not differ significantly. However, A-type transducers provide higher sensitivity and longer transducer waveform, which allows the examination of the multipulse interference of small signals. To further examine the possible influence of the transducer bandwidth, the wider bandwidth C-type transducers were analyzed. It is important to note that the design of the particular transducer is also evident in the results of the multipulse excitation. For instance, for the C-type transducers, the multipulse responses clearly exhibit two resonant peaks in their responses in agreement with their transfer functions.²⁴

Finally, as the effects of the transducer resonance are interpulse time delay dependent, we briefly consider the possible influence of pulse-to-pulse jitter on the effects' strength. Due to the bandwidth optimization of the USTs, the resonant peaks exhibited are quite broad. This relaxes the constraints on the precision of the interpulse delay required to perform resonant multipulse photoacoustic excitation. As we conclude from our experimental observations, a jitter in the order of 5 to 10 ns can be tolerated well. The pulse-to-pulse jitter of the DL systems is small comparable to that of the solid-state sources²⁵ and usually satisfies this limit well. Other possible sources of the variation of pulse-to-pulse arrival time might include changes associated with the temperature dependency of the speed of sound due to the heat deposition by the laser pulse. A higher boundary for the associated timing mismatch can be estimated based on the maximum temperature rise for a closely separated double-pulse excitation.²² Considering the maximum temperature change of a few degrees and limited heated volume, the upper boundary for the temperature-induced changes in the ultrasound time-of-flight is below 1 ns and, therefore, can be neglected.

To conclude the discussion, we quickly outline the implications the transducer resonances might have for the photoacoustic modalities. In photoacoustic tomography domain, the combination of pulse repetition rates and transducers used for advanced thermal methods²⁸ usually leads to interpulse delays allowing single-pulse responses to clear out, leading to no multipulse signal interference. However, when denser pulse sequences are used, the interference of the consecutive pulses present is superimposed over the nonlinearity of the Grueneisen relaxation effect, as visible from the supplementary material for Ref. 22.

In the recently introduced photoacoustic resonance imaging,¹⁵ operation in the pulse repetition rate close to matching the transducer resonances may present a source of ambiguity. When the photoacoustic signal generation chain is considered, the properties of the absorber and the transducer should be analyzed separately. Even if the illumination pattern is controlled, it is still not possible to distinguish the effects induced by the sample and the receiver if their behavior remains unknown. It is, therefore, instructive to search for possible separation of the absorber and the transducer resonances to be able to clearly identify and distinguish them.

Finally, the linearity of the combination of the individual signals even in the domain, when the pulse repetition rate is

approaching transducer resonances, is providing further room to use denser pulse sequences in coded excitation approach.^{16,17} This leads to the opportunity to further increase frame rates. Moreover, since the excitations with different t_R are filling the available transducer bandwidth independently,²⁴ it is possible to utilize simultaneous multiplexed multicolor excitation to further improve the acquisition time for multispectral imaging.

4 Conclusion

In this paper, we presented TM-MPE and analyzed the potential of this technique to increase the SNR in the systems possessing limited pulse energy.

We have shown experimentally and computationally that the maximum registered photoacoustic amplitude can be increased from 1.2 to 1.8 fold, dependent on the transducer and arrangement used. Since the SNR in PAI is linearly dependent on the registered amplitude, the mentioned improvement translates directly in the SNR gain. As the mechanisms of SNR increase for TM-MPE and ensemble averaging are different, both methods can be used in combination. This leads to the multiplication of the respective SNR gain factors. Thus, combining TM-MPE with averaging provides an alternative to either increase SNR keeping the total acquisition time, maintain SNR while increasing frame rate, or extract additional information using both single- and multipulse frames.

The analysis is performed for the regime of μJ pulse energies, where consecutive pulses interact primarily linearly at the transducer. Therefore, the results obtained can be used as lower estimate of the SNR improvement capabilities. The findings reported are of immediate interest to systems possessing limited pulse energy. In particular, this holds for DL-based systems and is of specific interest for applications using the transducers in the 1 to 5 MHz range (interpulse delay time t_R of 200 ns to 1 μs) since the necessary hardware is readily available.

Finally, the results reported are related to the recently introduced advanced PAI modalities,^{20,22} demonstrating that the effect of the transducer resonance has to be taken into account in the conditions where dense illumination patterns are used.

Disclosures

The authors declare no conflicts of interest.

Acknowledgments

The authors are grateful for the support of the Group for Medical Engineering at Ruhr University Bochum headed by professor Dr. Georg Schmitz. M.N.C. is grateful to OILTEBIA colleagues, speakers, and fellows for stimulating discussions. The authors acknowledge financial support by EU FP7 People: Marie Curie Actions; Award No. 317526 (OILTEBIA), and the DFG Open Access Publication Funds of the Ruhr University Bochum.

References

1. L. V. Wang and H.-I. Wu, *Biomedical Optics*, John Wiley & Sons, Inc., Hoboken, New Jersey (2009).
2. H. Jiang, *Photoacoustic Tomography*, CRC Press, Boca Raton, Florida (2014).
3. L. V. Wang, *Photoacoustic Imaging and Spectroscopy*, CRC Press, Boca Raton, Florida (2009).
4. T. J. Allen, B. T. Cox, and P. C. Beard, "Generating photoacoustic signals using high-peak power pulsed laser diodes," *Proc. SPIE* **5696**, 233–242 (2005).

5. K. Daoudi et al., "Handheld probe integrating laser diode and ultrasound transducer array for ultrasound/photoacoustic dual modality imaging," *Opt. Express* **22**, 26365 (2014).
 6. P. K. Upputuri and M. Pramanik, "Performance characterization of low-cost, high-speed, portable pulsed laser diode photoacoustic tomography (PLD-PAT) system," *Biomed. Opt. Express* **6**, 4118 (2015).
 7. S. K. Kalva, P. K. Upputuri, and M. Pramanik, "High-speed, low-cost, pulsed-laser-diode-based second-generation desktop photoacoustic tomography system," *Opt. Lett.* **44**, 81 (2019).
 8. F. Gao et al., "Single laser pulse generates dual photoacoustic signals for differential contrast photoacoustic imaging," *Sci. Rep.* **7**(1), 1–12 (2017).
 9. J. Diebold and M. I. Khan, "Photoacoustic 'signatures' of particulate matter: optical production of acoustic monopole radiation," *Science* **250**(4977), 101–104 (1990).
 10. G. J. Diebold, T. Sun, and M. I. Khan, "Photoacoustic monopole radiation in one, two, and three dimensions," *Phys. Rev. Lett.* **67**, 3384–3387 (1991).
 11. T. Liu et al., "Photoacoustic generation by multiple picosecond pulse excitation," *Med. Phys.* **37**(4), 1518–1521 (2010).
 12. R. Fuentes-Domínguez et al., "Size characterisation method and detection enhancement of plasmonic nanoparticles in a pump-probe system," *Appl. Sci.* **7**(8), 819 (2017).
 13. R. Fuentes-Domínguez et al., "Super-resolution imaging using nanobells," *Sci. Rep.* **8**(1), 16373 (2018).
 14. F. Gao et al., "Photoacoustic resonance spectroscopy for biological tissue characterization," *J. Biomed. Opt.* **19**(6), 067006 (2014).
 15. R. Zhang et al., "Photoacoustic resonance imaging," *IEEE J. Sel. Top. Quantum Electron.* **25**(1), 1–7 (2018).
 16. M. P. Mienkina et al., "Experimental evaluation of photoacoustic coded excitation using unipolar golay codes," *IEEE Trans. Ultrason. Ferroelectr. Freq. Control* **57**, 1583–1593 (2010).
 17. M. P. Mienkina et al., "Multispectral photoacoustic coded excitation imaging using unipolar orthogonal golay codes," *Opt. Express* **18**, 9076–9087 (2010).
 18. M. F. Beckmann and G. Schmitz, "Photoacoustic coded excitation using pulse position modulation," in *IEEE Int. Ultrason. Symp.*, IEEE, pp. 1853–1856 (2013).
 19. M. F. Beckmann, H.-M. Schwab, and G. Schmitz, "Optimized SNR simultaneous multispectral photoacoustic imaging with laser diodes," *Opt. Express* **23**(2), 1816 (2015).
 20. H. Zhong et al., "Review of low-cost photoacoustic sensing and imaging based on laser diode and light-emitting diode," *Sensors* **18**, 2264 (2018).
 21. C. R. Hill, J. C. Bamber, and G. R. Ter Haar, *Physical Principles of Medical Ultrasonics*, John Wiley & Sons, Ltd., Chichester, UK (2004).
 22. L. Wang, C. Zhang, and L. V. Wang, "Grueneisen relaxation photoacoustic microscopy," *Phys. Rev. Lett.* **113**, 174301 (2014).
 23. M. Cherkashin et al., "Dynamics of the photoacoustic response of single-element PZT transducers to pulse burst excitation," *Proc. SPIE* **10064**, 100641Q (2017).
 24. M. Cherkashin et al., "Linking transducer transfer function with multipulse excitation photoacoustic response," *Proc. SPIE* **10139**, 101391J (2017).
 25. M. Cherkashin et al., "Dynamics of double-pulse photoacoustic excitation," *Proc. SPIE* **9708**, 97084C (2016).
 26. T. Lee, Q. Li, and L. J. Guo, "Out-coupling of longitudinal photoacoustic pulses by mitigating the phase cancellation," *Sci. Rep.* **6**(1), 21511 (2016).
 27. P. L. M. J. van Neer et al., "Simple method for measuring phase transfer functions of transducers," in *IEEE Int. Ultrason. Symp.*, IEEE, pp. 1454–1457 (2010).
 28. Y. Zhou et al., "Thermal memory based photoacoustic imaging of temperature," *Optica* **6**, 198–205 (2019).
- Maxim N. Cherkashin** studied materials science at North-Caucasus State Technical University from 2006 to 2011. In 2011, he completed a five-month Erasmus Mundus with Professor Hofmann's Group for Photonics and Terahertz Technology (PTT) at Ruhr University Bochum. In 2012 to 2013, he studied at the Faculty of Biomedical Engineering, Bauman Moscow State Technical University. In 2013, he rejoined Professor Hofmann's group to work on his PhD with a focus on diode laser (DL)-based photoacoustics.
- Carsten Brenner** studied electrical engineering at Ruhr University Bochum from 2000 to 2005. In 2009, he obtained his PhD from Ruhr University Bochum conducting research on terahertz technology with DLs and was awarded with the Gert Massenbergs-Preis for outstanding dissertation in engineering. Since 2010, he is a postdoc at the Group for PTT, Ruhr University Bochum. His fields of research include advancement of terahertz technology and semiconductor laser applications, such as creation of short pulses, external resonators, and areas of application.
- Martin R. Hofmann** holds the chair for PTT, Ruhr University Bochum, Germany. He received his PhD from Philipps-Universität Marburg in 1994. From 1995 to spring 1996, he worked at the University College Cork, Ireland, at the Fondazione Ugo Bordoni, Rome, Italy, and at Tele Danmark Research, Hoersholm, Denmark. From 1996 to July 2001, he performed his habilitation at Philipps-Universität Marburg before he joined Ruhr University Bochum in 2001.